Available online at www.sciencedirect.com
ScienceDirect
Geochimica et Cosmochimica Acta 70 (2006) 5075–5088
Geochimica
www.elsevier.com/locate/gca

Molecular simulations of metal adsorption to bacterial surfaces

Kelly J. Johnson [a], Randall T. Cygan [b,*], Jeremy B. Fein [a]

[a] Department of Civil Engineering and Geological Sciences, University of Notre Dame, Notre Dame, IN 46556, USA
[b] Geochemistry Department, Sandia National Laboratories, Albuquerque, NM 87185-0754, USA

Received 30 September 2005; accepted in revised form 5 July 2006

Abstract

The atomic-scale interactions that occur between cations and the metal-binding cell wall components common to many gram-positive bacteria were investigated using molecular simulations techniques. We examined the adsorption of Cd and Pb onto peptidoglycan and teichoic acid components of the bacterial cell wall using classical energy force field methods. Within the framework of molecular mechanics and the Cerius^2 modeling software, we used energy minimization, conformational analysis, and molecular dynamics to examine the different components of the cell wall and to determine relative binding energies and structural configurations of the cell wall components, both with and without the metals present. Electronic structure calculations of representative metal–organic complexes validate the more practical classical methods required in simulating the large number of atoms associated with the cell wall components. The classical force field simulations were conducted in both gas phase and solvated periodic cells. Force field-based simulation techniques can adequately describe the interactions of Cd with the cell wall, defining both metal ion coordinations and binding distances. However, the classical force field approach is inconsistent in describing the observed Pb–cell wall interactions due to possible limitations in the force field parameters, the propensity for Pb to form hydroxides at circumneutral pH, or the dominance of other adsorption mechanisms.

1. Introduction

Bacterial surfaces can adsorb a wide range of aqueous metals (e.g., Beveridge and Murray, 1976; Beveridge and Koval, 1981; Mullen et al., 1989), thereby impacting the mobility of mass in many water–rock systems. In recent years, the adsorption of aqueous metal cations onto bacterial surfaces has been extensively studied using both laboratory and field techniques. However, most adsorption reactions have been modeled as bulk-partitioning processes, with the major concern being the amount of metal adsorbed to the adsorbent and not the specific site of adsorption or the mechanism of adsorption. Molecular simulation techniques can be used to better constrain the binding mechanisms involved in bacteria–metal interactions, thereby creating more powerful, flexible, and quantitative models to examine the effects of adsorption on mass transport.

A number of experimental approaches have been used recently to elucidate the molecular-scale controls for metal binding onto bacterial cell walls. Bulk adsorption measurements, involving both protons and aqueous metal cations, conducted as a function of pH and/or metal–bacteria concentration ratio, can be used to indirectly constrain the important adsorption reactions and to determine the equilibrium constants for those reactions (e.g., Fein et al., 1997; Cox et al., 1999; Martinez and Ferris, 2001; Ngwenya et al., 2003). More direct constraints on the metal–bacterial cell wall binding environment have been offered by X-ray absorption fine-structure spectroscopy (XAFS) investigations (e.g., Sarret et al., 1998; Kelly et al., 2001; Boyanov et al., 2003a; Templeton et al., 2003; Francis et al., 2004). X-ray absorption spectroscopy can provide excellent constraints on the first and second nearest neighbors to a metal of interest on the cell wall. However, this approach only yields an averaged view of what may be a complex binding environment consisting of numerous ligands and binding orientations. Molecular simulation methods have the potential to be a complementary third approach for

* Corresponding author. Fax: +1 505 844 7216.
E-mail address: rtcygan@sandia.gov (R.T. Cygan).

0016-7037/$ - see front matter © 2006 Elsevier Inc. All rights reserved.
doi:10.1016/j.gca.2006.07.028

studying metal–bacteria adsorption reactions, providing a more detailed and atomistic understanding of how metal cations interact with specific functional group types within the bacterial cell wall.

Molecular simulations have previously been applied to model components of the bacteria cell. However, these studies focused on the lipid bilayer of the cell wall, not the metal-binding macromolecules within the cell wall (Bandyophadhyay et al., 2001; Shelley et al., 2001a,b). For example, Shelley et al. (2001b) simulated the self-assembly of the lipid bilayer starting with a random configuration, providing insight into two different phospholipid phases. The lipid bilayer research utilized coarse-grained simulation models to demonstrate the properties of the layer, grouping individual atoms with similar functionality into one entity. This scaling process enables modeling of relatively large systems and has reasonably low computational cost. However, because of the simplifications, the approach describes only bulk processes as opposed to atomic level interactions.

Molecular modeling methods can be used to calculate the total potential energy of a molecular cluster or of a periodic system through either molecular mechanics or quantum mechanics. Molecular mechanics evaluates the interactions of individual atoms or molecules while quantum methods extend the simulation tools to the electron level, evaluating the electronic structure of the system. Molecular mechanics methods require analytical expressions to describe the potential energy as a function of atomic geometry (Cygan, 2001). The energy expressions are typically parameterized by experimental observation or quantum calculations. Through molecular mechanics methods, such techniques as energy minimization, conformational analysis, and molecular dynamics can be applied to a system of interest, for example those involving many hundreds and thousands of atoms of macromolecules representing a bacterial surface.

Molecular modeling studies of bacterial surfaces (e.g., lipopolysaccharide structures associated with the cell membranes of gram-negative bacteria) have been completed over the past decade (Kastowsky et al., 1992; Wang and Hollingsworth, 1996; Obst et al., 1997; Kotra et al., 1999; Lins and Straatsma, 2001; Shroll and Straatsma, 2003). These studies have used various levels of atomic abstractions and classical molecular mechanics to evaluate the structure and dynamics of the complex surfaces. Previous research includes Shroll and Straatsma (2003) employing classical molecular simulation techniques to model the adhesion of *Pseudomonas aeruginosa* to the mineral goethite, and Obst et al. (1997) examining the impact of Ca^{2+} on the lipopolysaccharide structure of *Escherichia coli*.

The objective of the present study was to use a classical molecular mechanics approach to identify the binding mechanisms involved in Cd and Pb adsorption onto two cell wall macromolecules that are thought to be the foci of metal binding in a number of gram-positive bacterial species. The cations Cd^{2+} and Pb^{2+} were chosen because previous laboratory and XAFS research of these ions characterizes the interaction of these specific metals with bacteria surfaces and their relevant functional groups (Fein et al., 1997; Boyanov et al., 2003a; Boyanov et al., 2003b; Templeton et al., 2003; Borrok and Fein, 2005). Also, Cd tends to form a relatively stable configuration at circumneutral pH, while the Pb behavior is more complex due to its $6s^2$ outer shell electronic configuration. The lone pair electrons are often stereochemically active and induce a strong deformation of divalent lead polyhedra (Galy et al., 1975; Esteban-Gómez et al., 2006). This allowed us to test the applicability of molecular simulations to describe increasingly complex metal–ligand interactions.

We used energy minimization methods to derive binding energies of metal–ligand complexes and we applied molecular dynamics (MD) simulations to analyze equilibrium structures, coordination, bond distances of metal–ligand complexes, and to derive radial distribution functions for correlation to XAFS observations. We also used molecular dynamics to study the solvation of metal–ligand complexes in water molecules and to compare the resulting structures to gas phase simulations of metal–cell wall complexes.

2. Cell wall characteristics

Our molecular simulations are focused on the metal-binding cell wall constituents of *Bacillus subtilis* (a common gram-positive soil bacterium) because both the biochemistry and the surface chemistry have been well characterized (Beveridge and Murray, 1980). However, titration experiments, XAFS, and attenuated total reflectance Fourier transform infrared (ATR-FTIR) spectroscopy show that most gram-positive and gram-negative cell walls contain similar metal binding functional groups (Beveridge and Murray, 1980; Fein et al., 1997; Yee and Fein, 2001; Borrok et al., 2004; Jiang et al., 2004). Therefore, the results of our study are likely to be widely applicable for understanding metal-binding onto a range of similar bacterial species.

The primary components of the gram-positive cell wall are peptidoglycan, teichoic acid, and teichuronic acid (Elwood and Tempest, 1969; Beveridge and Murray, 1980; Beveridge, 1999). All three constituents contain functional groups that, when deprotonated, can effectively bind metal cations. Peptidoglycan contains carboxyl, hydroxyl, and amine functional groups, teichoic acid includes phosphoryl groups, and teichuronic acid is similar to teichoic acid but contains carboxyl functional groups rather than the phosphoryl groups of teichoic acid. Gram-negative cell walls include a lesser amount of peptidoglycan than gram-positive cells and have a complex outer membrane but they do not include teichoic and teichuronic acid constituents (Beveridge, 1999). The outer membrane of gram-negative bacteria contains phospholipids, lipoproteins, lipopolysaccharides, and various proteins. The phospholipids have phosphoryl groups in the same local coordination environment as the phosphoryl groups in teichoic acid.

The peptidoglycan structure consists of two sugars, *N*-acetylglucosamine and *N*-acetylmuramic acid (NAG, NAM), with a side peptide chain attached to the NAM. The peptide chain includes four amino acid groups with the D-glutamic acid and the *meso*-diaminopimelic acid (DAP) containing the two carboxyl groups of interest for metal cation adsorption. Peptidoglycan constitutes up to 50% of the cell wall by weight (Beveridge and Murray, 1980; Graham and Beveridge, 1994). Teichoic acids comprise the other major portion of the gram-positive cell wall. Teichoic acid is a polymer of glycerol linked by phosphoryl groups, which are the active adsorption sites (Fig. 1); *d*-alanine may also be present in teichoic acid but is not shown in the figure. There are generally 20–30 residues present in a chain and teichoic acid can represent up to 70% of the dry weight of the cell wall (Elwood and Tempest, 1969). Teichoic acid is linked covalently to the peptidoglycan sugars by a linkage unit containing two sugars and a phosphoryl group. The phosphoryl group in the linkage unit may also be active in adsorption of cations (Araki and Ito, 1989).

The cell walls of gram-positive bacteria can exhibit a negative charge due to the deprotonation of the carboxyl, phosphoryl, and hydroxyl functional groups (Beveridge and Murray, 1980). At low pH, the functional groups located on the cell wall are mostly protonated, and, therefore, little to no metal adsorption occurs. As pH increases, the surface functional groups deprotonate successively, resulting in the overall negative charge on the cell wall and an increasing number of sites available for metal

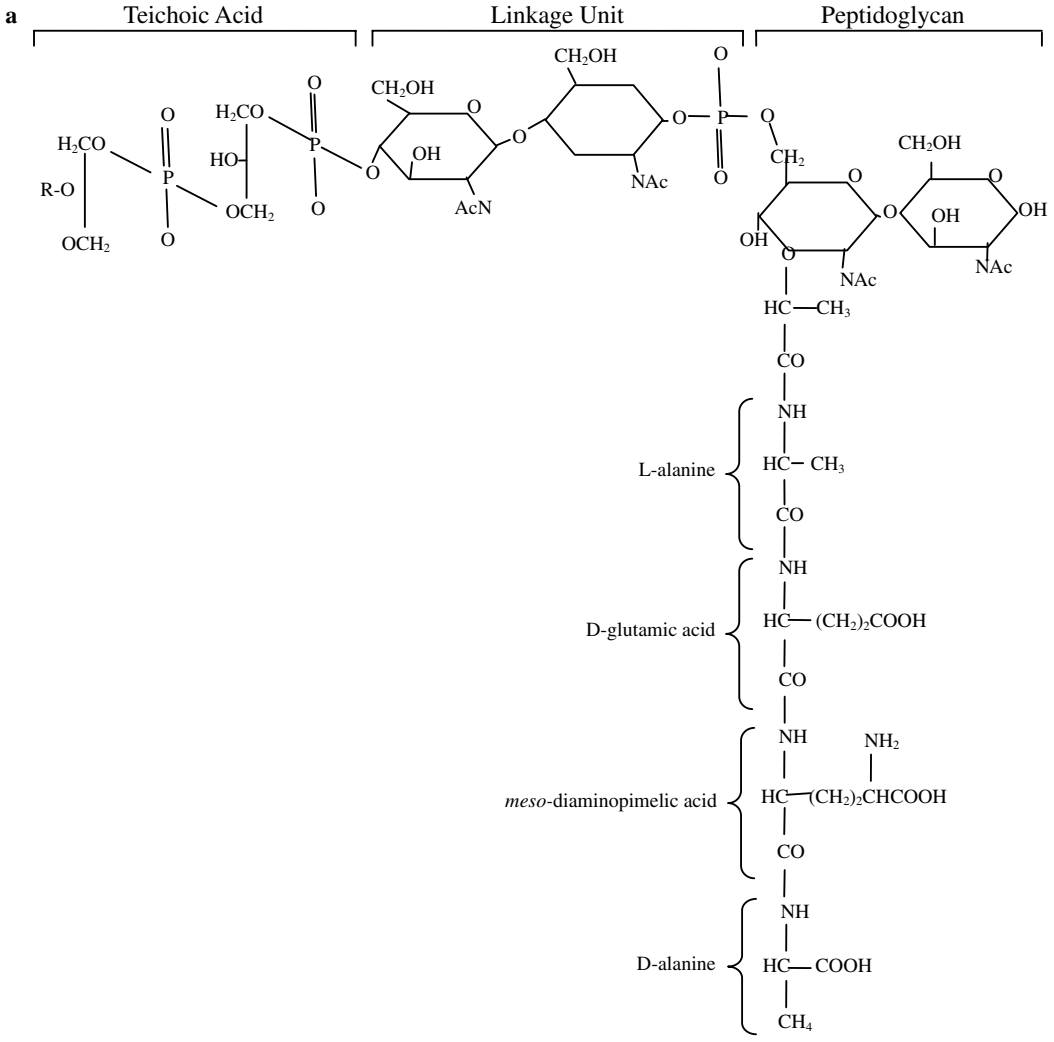

Fig. 1. The molecular simulation models developed from the schematic (a) of a peptidoglycan chain attached to a teichoic acid dimer. Peptidoglycan and teichoic acid are the major metal binding constituents of the *B. subtilis* cell wall at neutral pH. The optimized molecular model (b) is a representation of (a). Four peptidoglycan dimers were linked/bridged together to form more of a "fabric" representation of the cell wall (c). These structures were studied in gas phase simulations only due to their prohibitive size. Periodic simulation cells were used to study the effects of solvation on the interaction of the metal with the ligand. Initially the metal ion was placed in a periodic cell containing only water molecules (d). We also studied ligand–water associations (not shown) before placing both the metal and the ligand in the cell. Both (e) and (f) represent 1:2 metal:ligand stoichiometries. (e) Cd^{2+} associated with the peptidoglycan fragment and (f) Pb^{2+} with the teichoic acid. Both of these simulation cells contain more than 500 water molecules that have been removed to improve viewing of the metal–ligand complex.

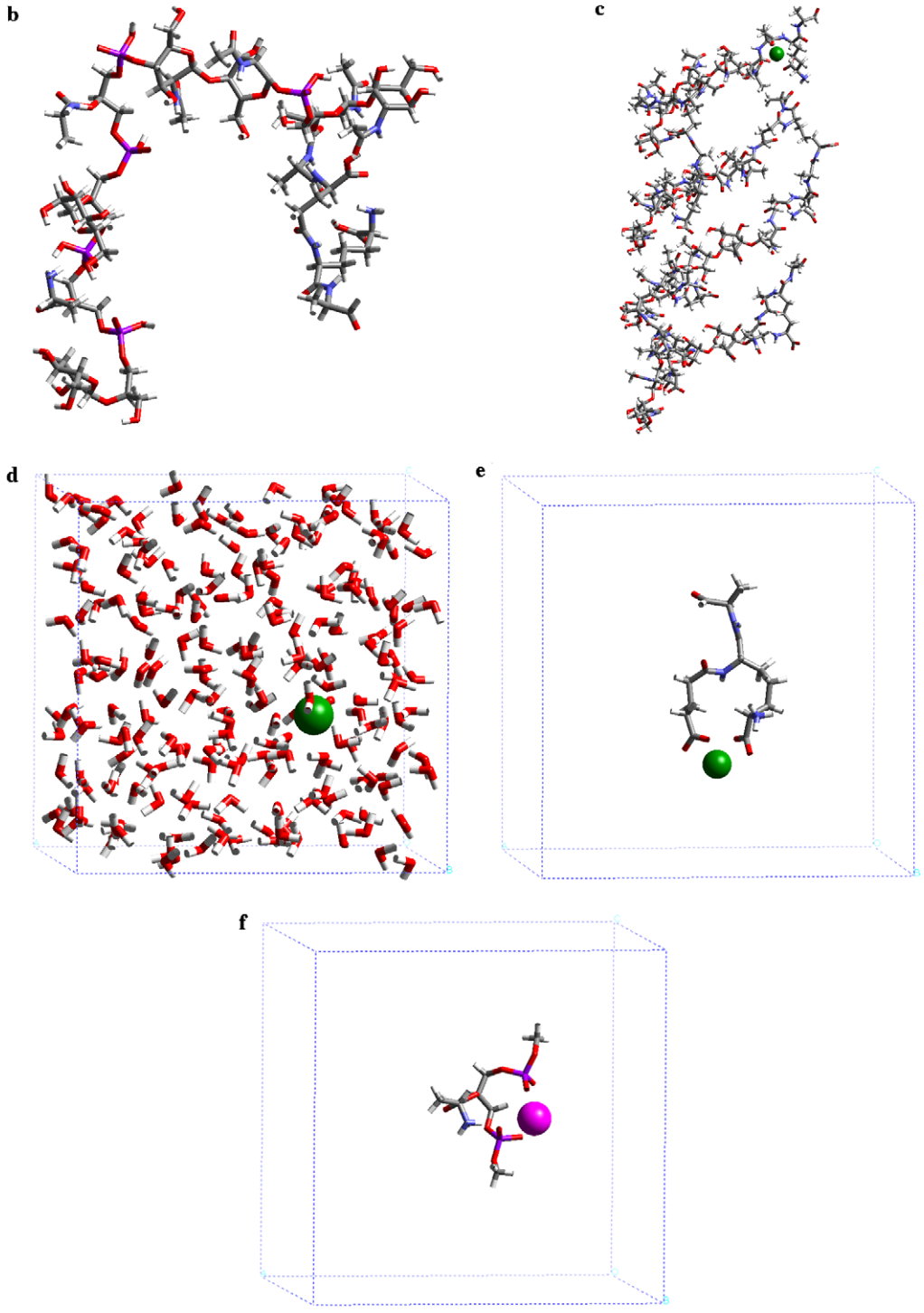

Fig. 1 (*continued*)

adsorption. Potentiometric titration experiments (e.g., Fein et al., 1997; Cox et al., 1999; Ngwenya et al., 2003; Fein et al., 2005) have shown these surface sites can be represented by discrete sites on the cell wall, each of which undergoes deprotonation according to the following reaction:

$$R\text{–}AH^0 \Longleftrightarrow R\text{–}A^- + H^+ \quad (1)$$

where R represents the bacterial cell wall macromolecule to which each functional group type, A, is attached. The pK_a values for the carboxylic and phosphoryl sites are 4.8 and 6.8, respectively, leading them to be deprotonated at circumneutral pH (Fein et al., 2005). Surface complexation modeling can be used to model bulk metal adsorption measurements assuming interaction between the deprotonated functional groups and the aqueous metal cations.

$$M^{m+} + R\text{–}COO^{-} \Longleftrightarrow R\text{–}COO(M)^{(m-1)+} \quad (2)$$

$$M^{m+} + R\text{–}PO^{-} \Longleftrightarrow R\text{–}PO(M)^{(m-1)+} \quad (3)$$

The equilibrium constants derived for reactions in this form can account for the observed adsorption behavior as a function of pH and bacteria–metal concentration ratio (see Fein, 2000 for a review of these approaches). In this molecular modeling study, we consider the interactions between aqueous Cd^{2+} and Pb^{2+} and deprotonated carboxylate and phosphoryl functional groups of the bacterial cell wall. We assume the valence electrons of the deprotonated functional groups to be delocalized between the two oxygen atoms.

3. Methods and model development

A series of molecular models of metal adsorption to the bacterial surface were developed using molecular simulation methods. Initial gas phase models of the macromolecules were created from published structures of peptidoglycan and teichoic acid (Beveridge and Murray, 1980; Araki and Ito, 1989; Navarre and Schneewind, 1999). These models were examined in different configurations to determine the optimal energy-minimized structures. Orientations of the molecular residues were systematically varied and then fully relaxed to obtain the global-minimized configuration. Next, a cation was placed proximate to a coordinating ligand and the new configuration was minimized by again allowing relaxation of all atoms. MD-based simulations were then conducted on the optimized gas phase metal–ligand models. Finally, solvation cells with periodic boundaries were developed to study the effect of full water solvation on metal–ligand interaction using MD simulations.

3.1. Simulation methods

Initial gas phase molecular simulations were used to graphically develop three-dimensional models of the peptidoglycan and teichoic acid molecules (Beveridge and Murray, 1980). The constant valence force field (CVFF) was applied to evaluate the interatomic potentials among the various atoms of the system. Through this force field, each atom has an assigned partial charge (Table 1) and a set of parameterized analytical functions to describe the potential energy of bonded and non-bonded interactions. All atomic positions were allowed to freely translate during each simulation; no constraints were imposed on the models. The CVFF force field was originally parameterized for applications involving peptide and protein structures by Dauber-Osguthorpe et al. (1988). The non-bonded parameters needed to describe the metal cations–ligand interactions are discussed below.

To model the critical intra-molecular interactions of the constituents of the cell wall, the potential energy of the system must be defined. The summation of the following energy components provides the total potential energy for the simulation:

Table 1
Partial charges of metal and ligand species used for molecular simulations

Metal	
Cd	2.0
Pb	2.0
Water	
H	0.41
O_W	−0.82
Carboxylate	
C	0.14
O_L	−0.57
Phosphoryl	
P	1.4
O_L	−0.85

$$E_{Total} = E_{Coul} + E_{VDW} + E_{BondStretch} + E_{Torsion} + E_{AngleBend} \quad (4)$$

The Coulombic and van der Waals energies represent the non-bonded terms, and the bond stretch, torsion, and angle bend correspond to the bonded interactions. The non-bonded terms control the binding and adsorption of the metal cation to the organic molecules, whereas the bonded terms generally describe the atomic configuration within the organic molecules. The E_{Coul} term accounts for the long-range electrostatic interactions and is represented by:

$$E_{Coul} = K \sum_{i \neq j} \frac{q_i q_j}{r_{ij}} \quad (5)$$

The partial charges q_i and q_j are typically obtained from quantum mechanics calculations, K is a constant, and r_{ij} is the distance between the two atoms of the summation. The van der Waals energy, E_{VDW}, represents the short-range interactions that prevent the overlap of atomic electronic clouds. It is represented by a Lennard-Jones function:

$$E_{VDW} = \sum_{i \neq j} D_o \left[\left(\frac{R_o}{r_{ij}} \right)^{12} - 2 \left(\frac{R_o}{r_{ij}} \right)^{6} \right] \quad (6)$$

where D_o and R_o are empirical parameters derived from the fitting of the potential energy model to observed structural and physical property data.

Values for the Lennard-Jones parameters for Cd and Pb interacting with oxygen Eq. (6) were previously unknown. We therefore chose to derive these potentials using an appropriate analog such as Ba^{2+} from the parameters of Åqvist (1990). Through a comparison of Åqvist Ba^{2+}, Åqvist Sr^{2+}, and Palmer Sr^{2+} (Åqvist, 1990; Palmer et al., 1996) Lennard-Jones parameters, we determined that Cd and Pb potentials derived from the Åqvist Ba^{2+} value were validated by consistent coordination numbers, solvation energies, and metal–ligand distances for both metal cations when comparing to experimentally determined values (Franks, 1973; Baes and Mesmer, 1976; Ohtaki et al., 1993). The Lennard-Jones parameters Eq. (6) for

Cd are $D_0 = 0.0470$ kcal/mol and $R_0 = 3.1011$ Å; and for Pb are $D_0 = 0.0470$ kcal/mol and $R_0 = 3.8364$ Å. Solvation energies for Cd and Pb derived from MD simulations using periodic water boxes (cation with 216 water molecules), as seen in Table 3, are −373.4 and −325.3 kcal/mol, respectively. These values are within 15% of the experimental solvation energy of Franks (1973), respectively, −436.9 kcal/mol and −359.0 kcal/mol.

Molecule models were optimized by first completing a series of energy minimizations (also referred to as geometry optimizations) to test various initial configurations and to obtain the most stable configuration for the molecules. Our initial modeling emphasized the simulation of isolated molecular clusters, or gas phase representations, of the cell wall components. Energy minimizations involve the repeated sampling of the potential energy surface until the potential energy minimum is obtained corresponding to a configuration where the forces on all atoms are zero (Cygan, 2001). Multiple initial structures were tested to ensure the true global energy minimum has been obtained and avoid any configuration corresponding to a local energy minimum. Minimizations are an important tool for examining energies as well as determining metal–ligand bond distances and coordination.

MD simulations were also utilized in this work to examine the significance of thermal processes on the energy-optimized molecular configuration. The MD method is a deterministic technique that allows the molecular system to evolve in response to a distribution of atomic motions and velocities dictated by the force field (Cygan, 2001). In dynamics simulations, Newton's equations of motion are iteratively solved for typically femtosecond time steps. MD simulations overcome some of the limitations associated with energy minimization by allowing the kinetic energy of the system to assist atoms in an improved sampling of the potential energy surface and leading to a thermally equilibrated configuration. From these dynamics simulations we can better assess equilibrium structures, coordinations, bond distances of metal–ligand complexes, and derive radial distribution functions for comparison to XAFS data. We can also examine the explicit solvation of metal–ligand complexes in water using periodic simulation cells. To create a periodic cell a peptidoglycan or teichoic acid sub-unit, a cation, and over 500 water molecules are placed in a simulation cell of appropriate size for the density of interest. Surface effects are eliminated by the three-dimensional periodic boundary conditions and the minimum image convention; the simulation cell is effectively surrounded in all directions by translated copies of itself. MD simulations were performed on a gas phase peptidoglycan monomer linked to a teichoic acid dimer (Pep-TA) and on solvated periodic cell structures of metal adsorption to either peptidoglycan or teichoic acid sub-units. The gas phase MD simulations were completed to ensure equilibrium was reached and to determine the average distances for cations adsorbed to the macromolecule. Solvation boxes containing both the metal and ligand were examined to obtain adsorption energies, metal coordination number, and ion–water and ion–organic binding distances.

Additionally, a series of gas phase electronic structure calculations was performed on a set of peptidoglycan and teichoic acid fragments (sub-units), identical to those used in the MD study of the hydrated periodic systems. The quantum simulations provide a critical independent check on the validity of the force field parameters, and provide a molecular orbital basis for describing the metal–organic interactions. Optimized configurations of the fragments with and without the metal cations were obtained using the all-electron density functional code Dmol[3] (Delley, 1990, 2000). Nonlocal gradient-corrected electron correlation (generalized gradient approximation) with double numerical plus polarization functionals was implemented (Perdew and Wang, 1992). A self-consistent field solution was obtained through iteration of the wave equations and an energy tolerance of 0.0063 kcal/mol. Geometry optimization of each system was obtained through a series of steepest descent, conjugate gradient, and Newton Raphson methods with full atomic relaxation and an energy convergence of 0.013 kcal/mol.

3.2. Model development

The Cerius[2] graphical-based molecular simulation software package (Accelrys, Inc., San Diego) was employed for the development of all molecular models. Energy, energy optimization, and molecular dynamics calculations were performed with the OFF energy software available within the modeling package. The CVFF force field was applied to the simple monomer representations of peptidoglycan and teichoic acid. The potential energy for each model was evaluated with a spline cutoff distance of 8.5 Å for the non-bonded van der Waals interactions and an Ewald summation for the periodic cells was used for the Coulombic interactions to ensure proper energy convergence (Tosi, 1964; Allen and Tildesley, 1987). As the result of charged systems in the periodic models (due to deprotonated functional groups and/or the presence of metal cations), a background screening correction was used to compensate excess charge and provide a neutral simulation cell.

Energy minimizations were performed on gas phase models to obtain the energy optimized configuration for each structure. Once the peptidoglycan and teichoic acid monomers were developed, they were linked to create dimers, peptidoglycan–teichoic acid structures (Fig. 1b), and a larger peptidoglycan strand (Fig. 1c). The optimized potential energies from these various structures were recorded and used to evaluate the metal–organic interactions based on the stability of the metal–ligand complexes.

3.3. Metal interactions

After obtaining energy-optimized models of the peptidoglycan and teichoic acid structures, the carboxylic and

phosphoryl functional groups of interest were deprotonated to represent a circumneutral pH; amino groups were subsequently protonated to reflect the pH conditions. The structures were further energy optimized and examined to ensure that a global energy minimum was attained. Once fully optimized, a Cd or Pb cation was placed at an arbitrary distance from each functional group of interest. The system was again minimized, resulting in a metal ion coordinated or adsorbed to a deprotonated functional group. By varying the initial metal position, we ensured an optimum final configuration that was confirmed by comparing the potential energy values. The binding energies for the metal–cell wall association were then derived by comparison of the potential energy of the cell wall macromolecule models with those models containing the macromolecule and its associated cation.

Dynamics simulations were used to evaluate the solvated interactions of metal with peptidoglycan and teichoic acid abstract models and water. Due to computational cost, the largest periodic box contained 512 water molecules, requiring a smaller organic model than the full peptidoglycan or teichoic acid macromolecule structures used for the gas phase calculations. To create the smaller abstract molecule, the ligands were terminated beyond the carbon group that followed the functional groups of interest.

MD simulations were performed by placing the organic ligands in a cubic simulation cell with a volume of approximately 5900 $Å^3$ (during molecular dynamics simulation the box length of approximately 18.1 Å changed by no more than 0.2 Å in any one dimension) with periodic boundary conditions allowing all atoms to have complete freedom to translate and cross cell boundaries if necessary (Fig. 1d–f). NPT canonical ensemble MD simulations were performed at 1 bar and 300 K using Nose–Hoover (Hoover, 1985) and Parrinello–Rahman (Parrinello and Rahman, 1981) methods to control temperature and pressure, respectively, of the simulation. The MD time step was 1 fs. Initially, the simulation cells are not at thermodynamic equilibrium, causing the temperature of the cell to significantly fluctuate during the first few picoseconds of the simulations. To avoid these thermal excursions and to obtain an equilibrated molecular configuration, a 30 ps equilibration run was first conducted, followed by a 50 ps production MD run. We observe this combination of dynamics simulations to be sufficient in allowing full system equilibration; potential and kinetic energies and temperature attained steady state values within this period. Dynamics trajectories representative of the equilibrated system were stored for only the last 30 ps of the total 80 ps simulation time. Radial distribution functions (RDF) can be derived from the atomic trajectories saved from the MD simulations. The RDF represents the distribution of distances between coordinating atoms during the simulation and can be compared directly with similar distributions derived from XAFS experimental data.

4. Results and discussion

4.1. Ligand model development and structural optimization

Energy-optimized models were obtained for a peptidoglycan monomer, teichoic acid monomer, dimers of both of these structures, a peptidoglycan monomer linked to a teichoic acid dimer (Pep-TA), and, finally, a larger strand of four linked peptidoglycan dimers. Each peptidoglycan monomer contains two carboxylate groups and each teichoic acid monomer contains two phosphoryl groups. During energy minimization of the Pep-TA, the carboxylate and phosphoryl groups did not interact with one another.

4.2. Ligands–M^{2+} energy minimization

Though the various models allow for full atomic and molecular flexibility, the structures of the peptidoglycan and teichoic acid remain relatively stable with little configurational change along the molecular chains when a cation is associated with the primary ligand. Most conformational change occurs in the orientation of the atoms within or near the deprotonated functional group to obtain the most favorable metal–ligand complex configuration. Because all atoms in the molecules possess a partial charge, ligand atoms located close to the cation respond by "moving" away (same charge) or closer to the cation (opposing charges) during the energy minimization. Deprotonation of the carboxyl and phosphoryl functional groups is pH related, therefore, these atomistic models allow for a better understanding of the response of the cell wall to both pH changes and cation interaction. Due to the static nature of the molecular models and the limitations of the nonreactive CVFF force field, the protonation state of the functional groups is assigned during model development, and therefore is fixed and does not change during the simulations.

4.2.1. Binding energies

Energy minimizations were conducted on peptidoglycan and teichoic acid structures in the presence of Cd and Pb. Initial calculations assumed the models to exist as isolated gas phase molecules, without incorporation of the effects of solvating water molecules. Studying the individual energies of the Pep-TA structure with and without the metal cations, we were able to compare the binding energies of the individual functional groups (Table 2). We use the term *binding energy* to represent the association energy of the metal complex reactions as described by Eqs. (2) and (3), where the negative sign indicates the stable formation of the complex. The derived binding energies should only be compared in a relative sense because of the limitations associated with any empirical force field like CVFF, and the introduction of specialized Lennard-Jones parameters for the metal cations. When compared to experimental values, the theoretical energies are typically an order of magnitude greater. These greater theoretical values are not

Table 2
Binding energies (kcal/mol) for Cd^{2+} and Pb^{2+} for the gas phase simulations of metal adsorption to the peptidoglycan ligand linked to the teichoic acid (Pep-TA)

Ligand	Cd^{2+}	Pb^{2+}
Carb-D	−381.3	−329.3
Carb-G	−453.4	−320.3
Carb-DG	−482.1	−398.8
Phos-L	−422.1	−359.2
1Phos	−430.8	−346.9
2Phos	−493.4	−463.2

The energies are obtained by subtracting the potential energy of the energy-minimized Pep-Ta structure and the free metal cation (0 kcal/mol) from the total potential energy when the ligand is associated with the cation. Carb-D, Carb-G, and Carb-DG denote which carboxylate ligand (*meso*-diaminopimelic acid and/or D-glutamic acid) the metal is associated with. Phos-L indicates the phosphoryl group that links the peptidoglycan and teichoic acid.

surprising owing to the lack of any solvating water molecules coordinating to the metal–ligand association. Note that binding energies derived from electronic structure calculations of the small-sized proxy metal–organic complexes are similar to those derived using the classical force field approach and those above for the larger cell wall models. The binding energies can be used to determine which cation is preferentially bound to the ligand of interest. The complexation of metal with two ligands provides a more negative binding energy for both Cd and Pb than complexing with one ligand, suggesting a 1:2 metal–ligand coordination is more stable as expected. Cd interaction with the two phosphoryl groups of the teichoic acid displays the most negative binding energy. For 1:1 metal–organic pairings, the glutamic acid carboxylate group exhibits the most negative binding energy for Cd, while the Pb binds more tightly to the phosphoryl group. The Cd modeling result is concurrent with the findings of Beveridge and Murray (1980) that the glutamic acid site on the peptidoglycan is the most apparent site for metal complexation on *B. subtilis*.

Cd displays a more negative binding energy than Pb for all adsorption sites, suggesting Cd is bound more tightly to the ligand than Pb. These results are inconsistent with trends observed in bulk adsorption laboratory studies, in which bacterial cell walls are observed to adsorb significantly more Pb than Cd under identical experimental conditions (e.g., Fein et al., 1997). The difference between our simulation models and the results of Fein et al. (1997) are likely due to hydration effects or the presence of covalent bonding between the metal cation and the organic ligand.

Results for electronic structure optimizations of the fragment representations of peptidoglycan and teichoic acid support those obtained from the classical simulations. Force field-based simulations of the identical fragment systems were used to compare the two different theoretical methods. The quantum simulations provide binding energies for the Cd–ligand and Pb–ligand complexes that are 25–80 kcal/mol stronger than the values obtained by the force field method; the mean relative difference between the two methods is approximately 14%. As observed for the large cell wall models, Cd binds more strongly than Pb with the peptidoglycan complexes with carboxylate ligands more favored than those involving the phosphoryl groups of teichoic acid. These results are consistent with either quantum or classical method. Comparison of the optimized metal complex structures is quite good with metal–ligand distances in agreement by less than 5% difference. All optimized structures exhibit the metal ions coordinated by four oxygen ligands. This coordination is most enhanced for the Cd–peptidoglycan complex where the two carboxylate groups form a more tightly bound and relatively planar coordination about the smaller Cd ion. Conformations of the organic backbone for the optimized structures derived using the two methods are in very good agreement with only subtle differences observed. Additionally, analysis of the electron density and molecular orbitals derived from the quantum calculations indicates predominantly spherical distributions about Pb and no strong evidence for the lone electron pair ($6s^2$) influencing the coordination environment for the Pb complexes.

4.2.2. Metal–oxygen distances

The metal cation–oxygen distances from the non-solvated gas phase MD models are dependent on the type of metal, the functional group, and the number of sites involved in the metal binding. In gas phase simulation Cd exhibits a shorter carboxylate binding distance than Pb, 2.19 versus 2.46 Å, respectively, correlating reasonably with the 2.3 and 2.5 Å values, respectively, of Franks (1973). The binding distances for the fully optimized structures are less than the observed values for both metals likely due to the gas phase simulations not addressing the effect solvation has on experimental systems. In addition, the metal–oxygen distances for metals complexing with two ligands are less than those for single ligand complexes due to increased electrostatic attractions.

4.3. Molecular dynamics of periodic hydrated systems

Five types of periodic systems were examined using MD to determine the binding energies of Cd and Pb to the peptidoglycan and teichoic acid fragments in hydrated periodic systems: metal only, ligand only, metal bound to two functional groups, metal bound to one functional group, and a cell containing the metal dissociated from the ligand. The metal and ligand only simulations were developed in order to differentiate their energetics from those simulations containing metal cations. Additionally, the matrix of simulations provides an opportunity to reduce the binding reaction to the fundamental components and energies. Each type of ligand–metal MD simulation was performed for Cd and Pb. The potential energy from the molecular simulations takes into account all atoms in the solvation box: the organic ligand, the metal ion, and water molecules. The energies (PE) reported in Table 3 for the

Table 3
Potential energy values for Cd^{2+} and Pb^{2+} from the molecular dynamics simulations for the periodic solvated metal–ligand structures

System	Model	Total PE (kcal/mol)	σ (kcal/mol)	Number of waters	PE/MLPE (kcal/mol)	σ MLPE (kcal/mol)	e_r (%)
Water	216 H_2O	−1965.0	20.5	216	−9.1	n/a	n/a
Cd–water	Cd–H_2O	−2338.4	22.8	216	−373.4	n/a	n/a
Pb–water	Pb–H_2O	−2290.3	22.5	216	−325.3	n/a	n/a
					MLPE		
Peptidoglycan fragment	Carb frag	−4752.5	35.2	508	−131.1	47.2	36.0
	Cd-1Carb	−5134.5	38.4	508	−513.1	49.7	9.7
	Cd-2Carb	−5179.7	40.3	512	−522.0	51.2	9.8
	Cd-Dis	−5123.1	39.5	508	−501.7	50.5	10.1
	Pb-1Carb	−5071.8	41.8	508	−450.4	52.3	11.6
	Pb-2Carb	−5118.6	39.4	512	−460.8	50.5	11.0
	Pb-Dis	−5125.7	36.4	512	−467.9	48.2	10.3
Teichoic acid fragment	Phos Frag	−4709.6	35.0	508	−88.2	47.1	53.4
	Cd-1Phos	−5086.7	30.2	508	−465.3	43.6	9.4
	Cd-2Phos	−5096.4	32.5	508	−475.0	45.2	9.5
	Cd-Dis	−5084.9	39.3	508	−463.5	50.4	10.9
	Pb-1Phos	−5037.0	37.8	508	−415.6	49.2	11.8
	Pb-2Phos	−5050.7	38.8	508	−429.3	49.9	11.6
	Pb-Dis	−5052.3	35.8	508	−431.0	47.7	11.1

The potential energies (PE) and metal–ligand potential energies (MLPE) are obtained by subtracting the potential energy of the water (the number of waters multiplied the self interaction energy of water) from the total potential energy of the simulation cell. σ MLPE denotes the standard deviation of the calculated MLPE and e_r (%) represents the percent of relative error. Cd-dis and Pb-dis denote simulations in which the cation was not adsorbed or associated directly with the ligand. The PE values for the Cd–water and Pb–water simulations are equivalent to the hydration enthalpy for the cation.

fragment simulations have significant relative error, and caution must be taken when trying to compare them to thermodynamic enthalpies.

In Table 3, metal–ligand potential energies (MLPE) were defined by subtracting the energy of the waters (the number of waters multiplied by the self interaction energy of water) from the total potential energy of the solvation box. The systems in which the metal was bound to two functional groups (either phosphoryl or carboxyl) resulted in lower potential energies for both Cd and Pb. For example, Pb interacting with two ligands (−460.8 kcal/mol) has a PE 10.4 kcal/mol lower than when it is interacting with one ligand (−450.4 kcal/mol). This energy difference is less than the standard deviation in the total PE for the MD simulations; nonetheless, this trend can be seen for both metals with both ligands.

The energy difference between the 1:1 and 1:2 metal–ligand stoichiometries reflects the greater stability achieved when the metal is coordinated to both functional groups. Boyanov et al. (2003a), using EXAFS analysis, were unable to determine if the metal–ligand stoichiometry is 1:1 or 1:2 for Cd–cell wall interactions due to overlapping error bars in their analysis, and therefore they based their structural models on a 1:1 stoichiometry. Fein et al. (1997) obtained better fits for their bulk Cd and Pb adsorption data using 1:1 metal–ligand stoichiometry and Boyanov et al. (2003b) observed a 1:1 Pb–carboxylate stoichiometry for their study of Pb adsorbed to a monolayer.

Similar to the gas phase simulations, the stabilization energies suggest that both peptidoglycan and teichoic acid components of the cell wall have a greater binding strength for Cd cations than for Pb. However, bulk adsorption studies have documented that the cell wall has a greater affinity for Pb than for Cd in both individual and competitive adsorption experiments (Fein et al., 1997; Fowle and Fein, 1999; Borrok and Fein, 2005). For example, Borrok and Fein (2005) conducted separate adsorption experiments in which 10 ppm of either Pb or Cd were reacted with 3 g/L *Pseudomonas mendocina*, a gram-negative bacterium. At pH 6.5, only half of the Cd was adsorbed onto the cell wall, while nearly all of the Pb was adsorbed under identical experimental conditions. The simulations presented here, therefore, must not fully describe the aspect of the binding mechanisms that account for the differences between Pb and Cd adsorption. The models also portray Pb binding the most strongly in systems where the cation is completely dissociated from the critical ligands, although these comparisons are associated with large uncertainty overlap. Our classical models account for the strength of metal adsorption through van der Waals and long-range electrostatic forces, but not explicit covalent effects. Also, differences in the tendency for Cd and Pb to form aqueous hydroxide complexes may influence the affinity for each metal to bind to the bacterial cell wall at near-neutral pH. The logarithm of the first hydrolysis constant for Cd and Pb is 3.9 and 6.3 (for the reaction stoichiometry of $M^{2+} + OH^- = MOH^+$; Baes and Mesmer, 1976), respectively, indicating that significant hydrolysis of Pb occurs under near-neutral conditions, while Cd-hydroxide formation does not occur to a significant extent except under higher pH conditions.

XAFS techniques have been used in various ways to investigate the adsorption of cations to the bacterial surface. Here, we compare XAFS results to the results of

MD simulations of Cd and Pb adsorption onto peptidoglycan and teichoic acid components of the bacterial cell to validate the molecular simulation models. In general, the radial distribution functions for cation–oxygen, cation–carbon and cation–phosphorous are similar for both Pb and Cd, with the overall peak shape and distribution being comparable for both metal cations (data not shown). As anticipated, the RDFs exhibit differences in mean distances and overall shape (distribution) of the curve. RDFs were calculated using the force field type for each of the atoms of interest, which allows us to discriminate the metal–oxygen distance for the metal–ligand complexes from that of the metal–water.

4.3.1. Cd^{2+} simulations

The first shell interactions of Cd–carboxylate complexation with both the oxygen of the peptidoglycan ligand and water oxygen in the solvated periodic systems can be compared in the RDF presented in Fig. 2. The highest peak shows the Cd–O distance for a 1:1 Cd–carboxylate complex is calculated to be 2.27 Å. When Cd is coordinated with two carboxylate groups the first shell is slightly expanded and the first peak maximum is at 2.33 Å. These metal cation–O_T (all oxygens; ligand and water) distances are both comparable to the 2.3 Å Cd–oxygen XAFS distances measured by Boyanov et al. (2003a). Analogous calculated Cd–oxygen distances for the 1:1 and 1:2 metal–ligand coordinations onto teichoic acid are 2.27 and 2.31 Å, respectively (Table 4). The XAFS measurements of Boyanov et al. (2003a) placed the first shell for Cd interacting with solution and the phosphoryl group oxygen of teichoic acid at 2.27 Å. Therefore the models for the interaction of Cd with the metal-binding macromolecules of the cell wall are consistent with the XAFS results.

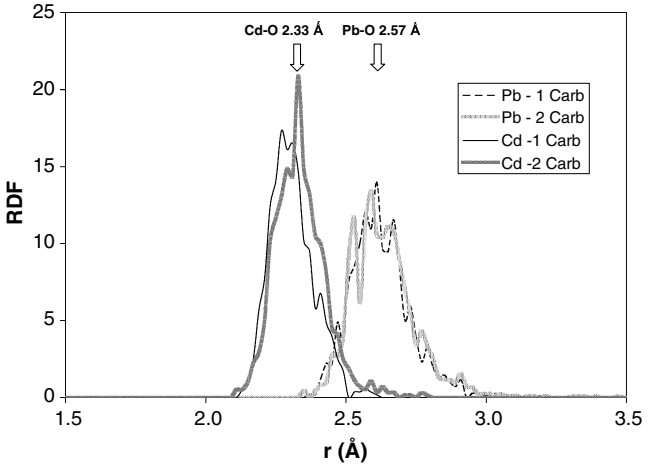

Fig. 2. Radial distribution functions from molecular dynamics simulations of M^{2+} interaction with the carboxylate ligand of the peptidoglycan fragment. The fine lines denote the RDFs for the 1:1 metal–ligand coordination and the thick lines are for the 2:1 metal–ligand coordination. The arrows indicate the simulated average metal–O_T distance for 1:2 coordination.

Analysis of the molecular simulation results help to differentiate between the ligand oxygen (O_L) and water oxygen (O_W) coordinated with the cation of interest in contrast to XAFS techniques where no chemical distinction can be made. This is helpful when attempting to differentiate among the various ligands coordinating to a metal either in solution or on a surface. Table 4 shows the average metal cation–oxygen distances for the different oxygen types and, similar to the RDFs, these results represent the average of the first coordination shell. While Cd is coordinated with one and two carboxylate ligands, the binding distances to the specific ligand oxygen are 2.27 and 2.33 Å, respectively. These are very close to the average metal cation–O_T distances, where O_T represents both ligand and water (total) oxygens. However, when binding with the phosphoryl groups of the teichoic acid, the 1:1 and 1:2 Cd–O distances are 2.19 and 2.13 Å, respectively. These distances are both smaller than the average metal cation–O_T distances for the Cd–phosphoryl group(s) interaction, which are 2.27 and 2.31 Å, respectively. Both the carboxylate and phosphoryl ligand sites have similar configurations, where an electron is delocalized between the two oxygen of the functional group. The Cd may be bound closer to the phosphoryl oxygen relative to the O_T due to the higher partial charge of the phosphoryl group oxygen (Table 1).

The Cd–peptidoglycan second coordination shell contains carbon at a distance of 2.63 Å from the metal for 1:1 stoichiometry and 2.67 Å for the 1:2 complex. For Cd complexation onto phosphoryl sites on teichoic acid, phosphorous is the second nearest neighbor at 2.99 and 2.95 Å (Table 4), respectively, for complexation with 1 and 2 phosphoryl groups. Boyanov et al. (2003a) fit their carboxylate data with a carbon shell at 2.7 Å and their teichoic acid with a phosphorus shell at 3.43 Å. Due to overlapping error bars XAFS could not be used to determine the Cd–carboxylate stoichiometry, as noted previously. The C-shell distance matches the XAFS results (within 2%), however, there is a sizeable shortening (approximately 13%) for the simulated Cd–P-shell distance with the one determined by XAFS.

Table 4 includes the coordination of the different atoms surrounding the Cd ion. To determine an average coordination value, the number of atoms surrounding the cation was counted and averaged every ten ps of the trajectory. X-ray scattering studies of solvated Cd have identified an octahedral hydration shell around the aqueous Cd^{2+} ion (Ohtaki et al., 1974; Caminiti et al., 1984; Marcus, 1988; Ohtaki and Radnai, 1993). In the molecular simulations Cd bound to two ligands was solvated by four water molecules and for single ligand coordination, the hydration sphere contained five water molecules. This inner sphere complex was seen by Boyanov et al. (2003a) in their XAFS models for Cd-*B. subtilis* experiments and also in X-ray scattering works on similar reference solutions (Caminiti and Johansson, 1981; Caminiti, 1982; Caminiti et al., 1984).

Table 4
The coordination and binding distances (Å) of cations with 1:1 and 1:2 metal–ligand stoichiometries derived from equilibrated NPT-ensemble molecular dynamics simulations of the hydrated peptidoglycan and teichoic acid fragments

Peptidoglycan					Teichoic acid				
Run	Shell	Avg CN	R	σ	Run	Shell	Avg CN	R	σ
Cd-2Carb	O_L	4	2.33	0.102	Cd-2Phos	O_L	3	2.13	0.339
	O_W	4	2.33	0.087		O_W	4	2.31	0.080
	C	2	2.67	0.074		P	2	2.95	0.317
	O_T	8	2.33	0.096		O_T	7	2.31	0.115
Cd-1Carb	O_L	2.2	2.27	0.086	Cd-1Phos	O_L	2	2.19	0.093
	O_W	5	2.29	0.076		O_W	5	2.33	0.075
	C	1	2.63	0.061		P	1	2.99	0.056
	O_T	7	2.27	0.080		O_T	7	2.27	0.086
Pb-2Carb	O_L	4	2.51	0.195	Pb-2Phos	O_L	3	2.45	0.117
	O_W	5	2.59	0.108		O_W	4.8	2.59	0.101
	C	2	2.93	0.113		P	2	3.19	0.338
	O_T	8.8	2.59	0.153		O_T	7.8	2.57	0.125
Pb-1Carb	O_L	2	2.55	0.121	Pb-1Phos	O_L	1	2.47	0.065
	O_W	6.6	2.61	0.104		O_W	7	2.59	0.126
	C	1	2.97	0.091		P	1	3.79	0.154
	O_T	8	2.61	0.111		O_T	8	2.59	0.140

O_L, carboxylate or phosphoryl oxygen; O_W, water oxygen; O_T, total oxygens; C, carboxylate carbon; and *P*, phosphoryl phosphorous.

Although XAFS methods cannot be used to differentiate between ligand and water oxygen, the agreement of the molecular simulations and XAFS results for the coordination numbers and distances of Cd with the cell wall sites is quite good. The correlation between these simulations, XAFS experiments, and laboratory experiments provide validation, at least to some extent, that the molecular simulations offer a reasonably accurate view of the adsorption of Cd and similarly behaving divalent cations onto the reactive cell wall components of a wide range of gram-positive bacteria. These results, along with the previous electronic structure validation, suggest that the force field and the Cd Lennard-Jones parameters derived from the Åqvist (1990) data set are sufficient for modeling these systems.

4.3.2. Pb^{2+} simulations

In the case of the Pb^{2+} ion, there are no XAFS data for direct comparison of Pb binding to the cell wall of gram-positive bacteria. However, there are other studies of Pb adsorption to gram-negative bacteria, fungal cells, and Langmuir monolayers, all containing carboxylate and phosphoryl functional groups (Sarret et al., 1998; Boyanov et al., 2003b; Templeton et al., 2003). Sarret et al. (1998) examined Pb binding to fungal cell walls, comparing carboxylate and phosphoryl complexes. Boyanov et al. (2003b) studied Pb adsorption to a fatty acid Langmuir monolayer that contained carboxylate head groups, and Templeton et al. (2003) applied XAFS to study adsorption and biomineralization within biofilms of the gram-negative bacteria *Burkholderia cepacia.* Although these various substrates lack the full-scale peptidoglycan and teichoic acid macromolecules, the binding of Pb to the carboxylate and phosphoryl functional groups can be compared to the molecular simulations of this study.

Our determinations for the average distances for Pb–oxygen in the first coordination shell are inconsistent with the experimental XAFS results. The calculated molecular simulation first shell Pb–O_T distances for 1:1 and 1:2 metal–ligand stoichiometries for carboxylate and phosphoryl group interactions are between 2.57 and 2.61 Å (Figs. 2 and 3). Although 2.59 Å is an average Pb–O distance for a hydrated Pb^{2+} cation (Franks, 1973), Templeton et al. (2003) found two distinct Pb–O distances of 2.30 ± 0.02 Å and 2.51 ± 0.02 Å with these distances being similar to Pb–O distances in lead organic model compounds determined by XAFS spectroscopy (Xia

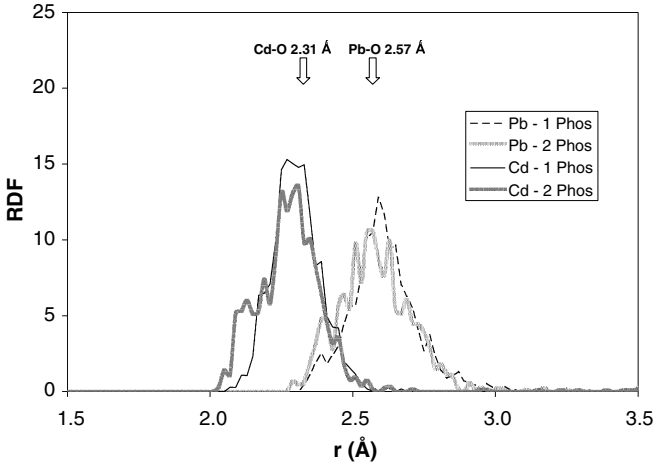

Fig. 3. Radial distribution functions from molecular dynamics simulations of M^{2+} interaction with the phosphoryl ligand of the teichoic acid fragment. The fine lines denote the RDFs for the 1:1 metal–ligand coordination and the thick lines are for the 2:1 metal–ligand coordination. The arrows indicate the simulated average metal–O_T distance for 1:2 coordination.

et al., 1997; Boyanov et al., 2003b). The shorter Pb–O distance and second neighbor Pb-(C, P) distance that Templeton et al. (2003) measured suggests the ligand forms an inner-sphere complex with the cation, while the longer Pb–O distance measured by the same group is consistent with outer-sphere aqueous Pb^{2+} complexes. However, in comparing our modeling results to spectroscopic data, it should be noted that obtaining correct first-shell interactions (Pb–O) is much more important than if second shell interactions (Pb–P, Pb–C) are similar, especially with such a unique element as Pb.

The calculated second shell interatomic distances for 1:1 and 1:2 Pb–C coordinations are 2.97 and 2.93 Å, respectively, for the peptidoglycan macromolecule. The calculated Pb–P distances for Pb bound to one and two phosphoryl groups of teichoic acid are 3.79 and 3.19 Å, respectively. The calculated Pb–C distances are the same as Boyanov et al. (2003b) found when looking at the interaction of Pb with the carboxylate groups on a Langmuir monolayer, and the Pb–P distance is similar to the 3.24 ± 0.04 Å Pb–P distance Templeton et al. (2003) measured for *B. cepacia*.

When coordinated with the phosphoryl group(s) of teichoic acid, the Pb is preferentially bound in a monodentate structure with oxygen, and when bound to both ligands the Pb interacted with three of the four oxygen ligands. This is a different result than observed by simulation for the Cd interaction when it was coordinated with one phosphoryl functional group where both ligand oxygens coordinated with the metal in a bidentate structure. Both Boyanov et al. (2003b) and Templeton et al. (2003) observed 1:1 stoichiometry for Pb–carboxylate and Pb–phosphoryl binding.

The simulations of Pb coordinated to one or two functional groups show the cation first coordination shell containing eight total oxygen atoms, with five to seven from the coordinating water molecules. The gas phase electronic structure simulations performed on the metal–ligand fragments support these force field results. The coordination of Pb with both oxygen and the respective C or P from the carboxylate or phosphoryl functional groups is difficult to discern using XAFS techniques due to the presence of the lone pair of electrons associated with the Pb^{2+} cation; this situation creates large disorder in the local coordination environment, particularly with organic complexes (Sarret et al., 1998). Both Boyanov et al. (2003b) and Templeton et al. (2003) observed Pb coordinated by four oxygen atoms. Our electronic structure calculations on the fragment models indicate substantially more transfer of electrons from the Pb (including the $6s^2$ lone pair) to the molecular bonding orbitals than observed for Cd; however, steric and conformational effects associated with the organic backbone while coordinating to the smaller ion contributed to a more stable Cd complex.

The molecular simulations for the adsorption of Pb onto the carboxylate and phosphoryl ligands of the peptidoglycan and teichoic acid molecules are consistent with some aspects of XAFS and surface complex modeling findings. Our calculated Pb–oxygen distances are in good agreement with experimental Pb–oxygen distances for a solvated Pb^{2+} cation, and the cation–P or cation–C distances are consistent. However, our simulations do not support the shorter inner-sphere Pb–oxygen bond distance measured by Templeton et al. (2003), or the Pb–O coordination observed by both Boyanov et al. (2003b) and Templeton et al. (2003). These discrepancies are perhaps the result of limitations in the force field approach or the existence of a different mechanism of adsorption for Pb to the cell wall. The classical-based models do not account for the transfer of electrons and the formation of covalent bonds associated with the Pb cation, or the ability of Pb to form hydroxide phases at circumneutral pH.

5. Conclusions

The results of the molecular simulations of this study can be used as a complement to surface complexation modeling and X-ray absorption spectroscopy for providing constraints on the nature of the binding mechanisms involved in cation adsorption onto bacterial surfaces. Using energy minimization and molecular dynamics simulations in this study, we modeled Cd^{2+} and Pb^{2+} adsorption onto the carboxylate and phosphoryl groups of peptidoglycan and teichoic acid that are present within the cell wall macromolecules of gram-positive bacteria. The force field-based models enable us to estimate the most stable complex configuration and compare binding affinities and interatomic distances with experimentally determined values to validate and predict metal cation adsorption behavior. MD simulations were incorporated to extend the molecular configurations derived from energy minimizations, and to model the influence of explicit water solvation of the organic components in the presence of solvated Cd and Pb cations.

The results of our molecular simulations of Cd–cell wall interactions indicate that molecular mechanics simulation techniques can adequately describe the interaction of Cd with the cell wall when comparing simulations with XAFS techniques and laboratory experiments. The molecular dynamics periodic cell simulations described both atom coordinations and binding distances that correlate very well with spectroscopic data. While simulations of Pb–ligand interactions do not agree with XAFS results as well as those obtained for the Cd models, their inconsistency can be construed as a need to refine force field parameters or to develop an alternative mechanism for Pb adsorption onto the cell wall.

The application of force field-based simulation methods allows us to examine relatively large and complex molecular systems such as the linked peptidoglycan dimers shown in Fig. 1c. These theoretical approaches are useful for studying the adsorption of a cation among multiple ligand sites, the rigidity of the major cell wall constituents, and adsorption strength, binding distance, and coordination number of various metal cations without the computational cost and limited system size required to use electronic

structure methods. Future research associated with molecular simulations of metal–bacteria interactions includes the development and refinement of force field parameters, development of larger representative cell wall models, analysis of multiple metal adsorption, and competitive adsorption processes.

Acknowledgments

Partial research funding was provided by a NSF Environmental Molecular Science Institute grant (EAR02-21966). K.J.J. was partially funded through a Bayer Predoctoral Fellowship in Environmental Science. We thank the US Department of Energy, Office of Basic Energy Sciences for funding to R.T.C. and K.J.J. through the Environmental Molecular Science Institute program. Sandia is a multiprogram laboratory operated by Sandia Corporation, a Lockheed Martin Company for the United States Department of Energy's National Nuclear Security Administration under Contract DE-AC04-94AL85000. We thank Louise Criscenti for helpful discussions regarding molecular model development, and Mike Machesky, Udo Becker, and two anonymous reviewers for their constructive criticism of an earlier version of the manuscript. Patricia Maurice and Peter Burns also provided valuable constructive comments on a draft of the manuscript.

Associate editor: Michael L. Machesky

References

Allen, M.P., Tildesley, D.J., 1987. *Computer Simulation of Liquids*. Oxford University Press, Oxford, 385 p.

Åqvist, J., 1990. Ion–water interaction potentials derived from free energy perturbation simulations. *J. Phys. Chem.* **94**, 8021–8024.

Araki, Y., Ito, E., 1989. Linkage units in cell walls of gram-positive bacteria. *Crit. Rev. Microbiol.* **17**, 121–135.

Baes, C.F., Mesmer, R.E., 1976. *The Hydrolysis of Cations*. Wiley.

Bandyophadhyay, S., Shelley, J.C., Klein, M.L., 2001. Molecular dynamics study of the effect of surfactant on a biomembrane. *J. Phys. Chem. B* **105**, 5979–5986.

Beveridge, T.J., 1999. Structures of gram-negative cell walls and their derived membrane vesicles. *J. Bacteriol.* **181**, 4725–4733.

Beveridge, T.J., Koval, S.F., 1981. Binding of metals to cell envelopes of *Escherichia-coli*-K-12. *Appl. Environ. Microbiol.* **42**, 325–335.

Beveridge, T.J., Murray, R.G.E., 1976. Uptake and retention of metals by cell walls of *Bacillus subtilis*. *J. Bacteriol.* **127**, 1502–1518.

Beveridge, T.J., Murray, R.G.E., 1980. Sites of metal deposition in the cell wall of *Bacillus subtilis*. *J. Bacteriol.* **141**, 876–887.

Borrok, D.M., Fein, J.B., 2005. The impact of ionic strength on the adsorption of protons, Pb, Cd, and Sr onto the surfaces of Gram negative bacteria: testing non-electrostatic, diffuse, and triple-layer models. *J. Colloid Interface Sci.* **286**, 110–126.

Borrok, D., Fein, J.B., Kulpa, C.F., 2004. Proton and Cd sorption onto natural bacteria consortia: testing universal adsorption behavior. *Geochim. Cosmochim. Acta* **68**, 3231–3238.

Boyanov, M.I., Kelly, S.D., Kemner, K.M., Bunker, B.A., Fein, J.B., Fowle, D.A., 2003a. Adsorption of cadmium to *Bacillus subtilis* bacterial cell walls: a pH-dependent X-ray adsorption fine structure spectroscopy study. *Geochim. Cosmochim. Acta* **67**, 3299–3311.

Boyanov, M.I., Kmetko, J., Shibata, T., Datta, A., Dutta, P., Bunker, B.A., 2003b. Mechanism of Pb adsorption to fatty acid Langmuir monolayers studied by X-ray adsorption fine structure spectroscopy. *J. Phys. Chem. B* **107**, 9780–9788.

Caminiti, R., 1982. Nickel and cadmium phosphates in aqueous solution-cation–anion complex formation and phosphate–H_2O interaction. *J. Chem. Phys.* **77**, 5682–5686.

Caminiti, R., Johansson, G., 1981. On the structures of cadmium sulfate complexes in aqueous solutions. *Acta Chem. Scand. Ser. A* **35**, 373–381.

Caminiti, R., Cucca, P., Radnai, T., 1984. Investigation on the structure of cadmium nitrate aqueous solutions by X-ray diffraction and Raman Spectroscopy. *J. Phys. Chem.* **88**, 2382–2386.

Cox, J.S., Smith, D.S., Warren, L.A., Ferris, F.G., 1999. Characterizing heterogeneous bacterial surface functional groups using discrete affinity spectra for proton binding. *Environ. Sci. Technol.* **33**, 4515–4521.

Cygan, R.T., 2001. Molecular modeling in mineralogy and geochemistry. In: Cygan, R.T., Kubicki, J.D. (Eds.), *Reviews in Mineralogy and Geochemistry: Molecular Modeling Theory: Applications in the Geosciences*. The Geochemical Society, Washington, DC, pp. 1–35.

Dauber-Osguthorpe, P., Roberts, V.A., Osguthorpe, D.J., Wolff, J., Genest, M., Hagler, A.T., 1988. Structure and energetics of ligand-binding to proteins: *Escherichia coli* dihydrofolate reductase trimethoprim, a drug–receptor system. *Proteins* **4**, 31–47.

Delley, B., 1990. An all-electron numerical method for solving the local density functional for polyatomic molecules. *J. Chem. Phys.* **92**, 508–517.

Delley, B., 2000. From molecules to solids with the $DMol^3$ approach. *J. Chem. Phys.* **113**, 7756–7764.

Elwood, D.C., Tempest, D.W., 1969. Control of teichoic acid and teichuronic acid biosynthesis in chemostat cultures of *Bacillus subtilis* var. niger. *Biochem. J.* **111**, 1–5.

Esteban-Gómez, D., Platas-Iglesias, C., Enríquez-Pérez, T., Avecilla, F., de Blas, A., Rodriguez-Blas, T., 2006. Lone-pair activity in lead(II) complexes with unsymmetrical lariat ethers. *Inorg. Chem.* **45**, 5407–5416.

Fein, J.B., 2000. Quantifying the effects of bacteria on adsorption reactions in water–rock systems. *Chem. Geol.* **169**, 265–280.

Fein, J.B., Daughney, C.J., Yee, N., Davis, T.A., 1997. A chemical equilibrium model for metal adsorption onto bacterial surfaces. *Geochim. Cosmochim. Acta* **61**, 3319–3328.

Fein, J.B., Boily, J.F., Yee, N., Gorman-Lewis, D., Turner, B.F., 2005. Potentiometric titrations of *Bacillus subtilis* cells to low pH and a comparison of modeling approaches. *Geochim. Cosmochim. Acta* **69**, 1123–1132.

Fowle, D.A., Fein, J.B., 1999. Competitive adsorption of metal cations onto two gram positive bacteria: testing the chemical equilibrium model. *Geochim. Cosmochim. Acta* **63**, 3059–3067.

Francis, A.J., Billow, J.B., Dodge, C.J., Harris, R., Beveridge, T.J., Papenguth, H.W., 2004. Uranium association with halophilic and non-halophilic bacteria and archaea. *Radiochim. Acta* **92**, 481–488.

Franks, F. (Ed.), 1973. *Water: A Comprehensive Treatise. V.3. Aqueous Solutions of Simple Electrolytes*. Plenum Press, New York.

Galy, J., Meunier, G., Andersson, S., Åström, A., 1975. Stéréochimie des eléments comportant des paires non liées: Ge(II), As(III), Se(IV), Br(V), Sn(II), Sb(III), Te(IV), I(V), Xe(VI), Tl(I), Pb(II), et Bi(III) (oxydes, fluorures et oxyfluorures). *J. Solid State Chem.* **13**, 142–159.

Graham, L.L., Beveridge, T.J., 1994. Structural differentiation of the *Bacillus subtilis* 168 cell wall. *J. Bacteriol.* **176**, 1413–1421.

Hoover, W.G., 1985. Canonical dynamics: equilibrium phase space distributions. *Phys. Rev. A* **31**, 1695–1697.

Jiang, W., Saxena, A., Song, B., Ward, B.B., Beveridge, T.J., Myneni, S.C.B., 2004. Elucidations of functional groups on gram-positive and gram-negative bacterial surfaces using infrared spectroscopy. *Langmuir* **20**, 11433–11442.

Kastowsky, M., Gutberlet, T., Bradaczek, H., 1992. Molecular modeling of the three-dimensional structure and conformational flexibility of bacterial lipopolysaccharide. *J. Bacteriol.* **174**, 4798–4806.

Kelly, S.D., Boyanov, M.I., Bunker, B.A., Fein, J.B., Fowle, D.A., Yee, N., Kemner, K.M., 2001. XAFS determination of the bacterial cell wall functional groups responsible for complexation of Cd and U as a function of pH. *J. Synchrotron Radiat.* **8**, 946–948.

Kotra, L.P., Golemi, D., Amro, N.A., Liu, G.Y., Mobashery, S., 1999. Dynamics of the lipopolysaccharide assembly on the surface of *Escherichia coli*. *J. Chem.* **38**, 8707–8711.

Lins, R.D., Straatsma, T.P., 2001. Computer simulation of the rough lipopolysaccharide membrane of *Pseudomonas aeruginosa*. *Biophys. J.* **81**, 1037–1046.

Marcus, Y., 1988. Ionic radii in aqueous solutions. *Chem. Rev.* **88**, 1475–1498.

Martinez, R.E., Ferris, F.G., 2001. Chemical equilibrium modeling: techniques for the analysis of high-resolution bacterial metal sorption data. *J. Colloid Interface Sci.* **243**, 73–80.

Mullen, M.D., Wolf, D.C., Ferris, F.G., Beveridge, T.J., Flemming, C.A., Baily, G.W., 1989. Bacterial sorption of heavy metals. *Appl. Environ. Microbiol.* **55**, 3143–3149.

Navarre, W.W., Schneewind, O., 1999. Surface proteins of gram-positive bacteria and mechanisms of their targeting to the cell wall envelope. *Microbiol. Mol. Biol. Rev.* **63**, 174–229.

Ngwenya, B.T., Sutherland, I.W., Kennedy, L., 2003. Comparison of the acid–base behaviour and metal adsorption characteristics of a gram-negative bacterium and other strains. *Appl. Geochem.* **18**, 527–538.

Obst, S., Kastowsky, M., Bradaczek, H., 1997. Molecular dynamics simulations of six different fully hydrated monomeric conformers of *Escherichia coli* re-lipopolysaccharide in the presence and absence of Ca^{2+}. *Biophys. J.* **72**, 1031–1046.

Ohtaki, H., Maeda, M., Ito, S., 1974. X-ray diffraction studies of aqueous solutions of cadmium perchorlate and sodium tetraiodocadmate. *Bull. Chem. Soc. Jpn* **47**, 2217–2221.

Ohtaki, H., Radnai, T., 1993. Structure and dynamics of hydrated ions. *Chem. Rev.* **93**, 1157–1204.

Palmer, B.J., Pfund, D.M., Fulton, J.L., 1996. Direct modeling of EXAFS spectra from molecular dynamics simulations. *Phys. Chem.* **100**, 13393–13398.

Parrinello, M., Rahman, A., 1981. Polymorphic transitions in single crystals: a new molecular dynamics method. *Appl. Phys.* **52**, 7182–7190.

Perdew, J.P., Wang, Y., 1992. Accurate and simple analytic representation of the electron-gas correlation energy. *Phys. Rev. B: Condensed Matter* **45**, 13244–13249.

Sarret, G., Manceau, A., Spadini, L., Roux, J.C., Hazemann, J.L., Soldo, Y., Eybert-Berard, L., Menthonnex, J.J., 1998. Structural determination of Zn and Pb binding sites in *Penicillium chrysogenum* cell walls by EXAFS spectroscopy. *Environ. Sci. Technol.* **32**, 1648–1655.

Shelley, J.C., Shelley, M.Y., Reeder, R.C., Bandyopadhyay, S., Klein, M.L., 2001a. A coarse grain model for phospholipid simulations. *J. Phys. Chem. B* **105**, 4464–4470.

Shelley, J.C., Shelley, M.Y., Reeder, R.C., Bandyopadhyay, S., Moore, P.B., Klein, M.L., 2001b. Simulations of phospholipids using a coarse grain model. *J. Phys. Chem. B* **105**, 9785–9792.

Shroll, R.M., Straatsma, T.P., 2003. Molecular basis for microbial adhesion to geochemical surfaces: computer simulation of *Pseudomonas aeruginosa* adhesion to goethite. *Biophys. J.* **84**, 1765–1772.

Templeton, A.S., Trainor, T.P., Spormann, A.M., Newville, M., Sutton, S.R., Dohnalkova, A., Gorby, Y., Brown, G.E., 2003. Sorption versus biomineralization of Pb(II) within *Burkholderia cepacia* biofilms. *Environ. Sci. Technol.* **37**, 300–307.

Tosi, M.P., 1964. Cohesion of ionic solids in the Born model. *Solid State Phys.* **131**, 533–545.

Wang, Y., Hollingsworth, R.I., 1996. An NMR spectroscopy and molecular mechanics study of the molecular basis for the supramolecular structure of lipopolysaccharides. *Biochemistry* **35**, 5647–5654.

Xia, K., Bleam, W., Hemke, P.A., 1997. Studies of the nature of Cu^{2+} and Pb^{2+} binding sites in soil humic substances using X-ray adsorption spectroscopy. *Geochim. Cosmochim. Acta* **61**, 2211–2221.

Yee, N., Fein, J.B., 2001. Cd adsorption onto bacterial surfaces: a universal adsorption edge? *Geochim. Cosmochim. Acta* **65**, 2037–2042.